Atten Percept Psychophys
DOI 10.3758/s13414-014-0650-2

Contrasting accounts of direction and shape perception in short-range motion: Counterchange compared with motion energy detection

Joseph Norman · Howard Hock · Gregor Schöner

Abstract It has long been thought (e.g., Cavanagh & Mather, 1989) that first-order motion-energy extraction via space-time comparator-type models (e.g., the elaborated Reichardt detector) is sufficient to account for human performance in the short-range motion paradigm (Braddick, 1974), including the perception of reverse-phi motion when the luminance polarity of the visual elements is inverted during successive frames. Human observers' ability to discriminate motion direction and use coherent motion information to segregate a region of a random cinematogram and determine its shape was tested; they performed better in the same-, as compared with the inverted-, polarity condition. Computational analyses of short-range motion perception based on the elaborated Reichardt motion energy detector (van Santen & Sperling, 1985) predict, incorrectly, that symmetrical results will be obtained for the same- and inverted-polarity conditions. In contrast, the counterchange detector (Hock, Schöner, & Gilroy, 2009) predicts an asymmetry quite similar to that of human observers in both motion direction and shape discrimination. The further advantage of counterchange, as compared with motion energy, detection for the perception of spatial shape- and depth-from-motion is discussed.

Keywords Short-range motion · Motion energy detection · Counterchange · Reverse-phi

J. Norman (✉) · H. Hock
Center for Complex Systems and Brain Sciences, Florida Atlantic University, Boca Raton, FL, USA
e-mail: joe.w.norman@gmail.com

H. Hock
Department of Psychology, Florida Atlantic University, Boca Raton, FL, USA

G. Schöner
Institut für Neuroinformatik, Ruhr-Universität Bochum, Bochum, Germany

Published online: 15 March 2014

Introduction

In an ecological context, many organisms benefit from minimizing their visual profile via camouflage in order to remain undetected (Stevens & Merilaita, 2009). As a coevolutionary complement, organisms have been selected with visual systems that are, at least in some cases, able to overcome the challenges in detecting and segregating entities whose static visual cues are obscured by camouflage. One basis for the perceptual "breaking" of camouflage entails the detection of coherent motion, which provides the opportunity to group portions of the visual field into connected wholes (as in the Gestalt principle of common fate) and to thereby segregate a moving entity from its background in order to determine its shape[1] from its motion. The short-range motion paradigm (Braddick, 1974), in which portions of a random field of elements are coherently displaced, provides a means for studying this ability to detect and segregate entities from their surrounding environment by virtue of their motion alone.

In the original two-frame short-range motion paradigm (Fig. 1), each square element of a random checkerboard has a .5 chance of being white (or black). A segment of the random checkerboard that is presented during the first frame is rigidly displaced and re-presented during the second frame (the coherent figure), while the surrounding elements are independently regenerated (the incoherent ground). Because the figure and background portions are generated in the same manner, the displaced figure is not detectable within individual frames on the basis of static cues; the perception of coherent motion is necessary in order to segregate the figure from the random, incoherently moving background elements and, thereby, determine its shape. As the size of

[1] By shape, we mean the ability to discriminate the orientation of the displaced figure. Although this does not put an explicit emphasis on the boundaries of the figure, they can be perceived at small displacements.

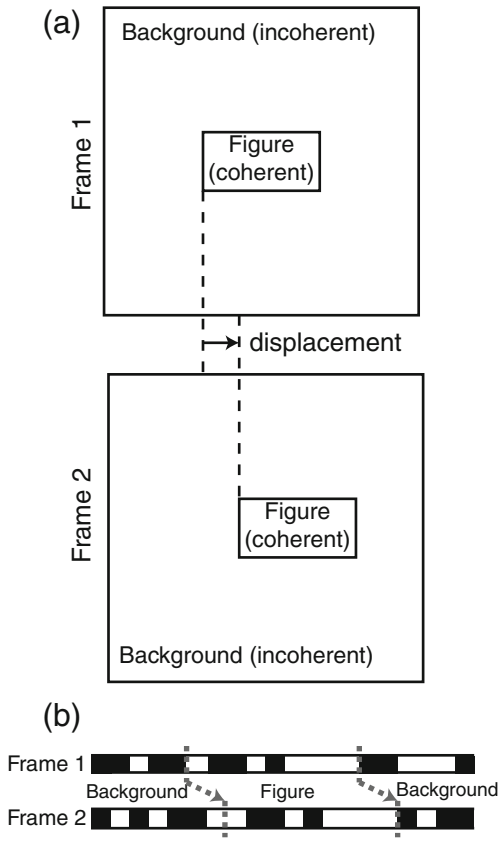

Fig. 1 Sketch of the two-frame short-range motion stimulus. The figure region is coherently displaced (either left or right) from frame 1 to frame 2, while the incoherent dynamic background is updated randomly. **a** Layout of the two-dimensional experimental stimulus. **b** A one-dimensional slice of the random dot cinematogram (with fewer dots than in the experiment). The stimulus used for the simulations below is also of the one-dimensional form depicted in panel b

the frame-to-frame displacement of the figure is increased, perceptual judgments become less consistent, with participants reporting a loss in coherence of the moving figure (Braddick, 1974; Sato 1989).[2] In this article, psychophysical experiments and computational simulations investigate the motion mechanisms that are the basis, in the two-frame short-range motion paradigm, for the perception of motion, the conditions under which it is coherent enough to segregate a moving figure from its background, and the perception of the figure's shape from the coherent motion.

Short-range motion perception has been considered a paradigmatic case for motion energy detection[3] (Adelson & Bergen, 1985; Cavanagh & Mather, 1989; Marr & Ullman, 1981; van Santen & Sperling, 1985). A major feature of models of Fourier-based motion energy detection (Adelson & Bergen, 1985; van Santen & Sperling, 1985) is that they predict reverse-phi motion (Anstis, 1970). As is shown in Appendix 2, motion is predicted in the direction opposite to that of the displacement when the luminance polarity of the visual elements composing a stimulus is inverted between successive frames (i.e., white elements become black and black elements become white). The strength of this reverse-phi motion is identical to the strength of motion in the direction of displacement when luminance polarity remains the same. Consequently, empirical evidence for asymmetry in motion and shape perception between the same- and inverted-polarity stimuli would indicate that motion perception was not determined solely by motion energy detection.

Experimental results relevant to this determination have been reported by Sato (1989), who tested both direction of motion and shape discrimination with both same- and inverted-polarity versions of the short-range motion stimulus. Although he reported that direction discrimination was similar for the same- and inverted polarity stimuli, this symmetry was not consistently obtained in all his experiments. Whenever performance was below ceiling, direction discrimination was poorer for inverted-polarity stimuli. Moreover, shape discrimination was severely deteriorated for the inverted-polarity stimuli, regardless of the size of the displacement. If these asymmetries were empirically confirmed, it would provide evidence that motion perception and the perception of shape from motion in the short-range paradigm are not primarily determined by first-order motion energy detectors. Instead, or in addition, an alternative motion detection mechanism that is sensitive to the difference between same- and inverted-polarity stimuli would be implicated. The alternative mechanism that is evaluated here entails the detection of counterchange—that is, oppositely signed changes in activation for pairs of spatial filters at different spatial locations (Hock, Gilroy, & Harnett, 2002; Hock, Schöner, & Gilroy, 2009).

Because the symmetry, or lack thereof, of motion and shape perception in same- and inverted-polarity conditions is theoretically critical, the present study begins with a psychophysical experiment that reevaluates and extends Sato's (1989) results. Computational simulations then determine how well the results obtained in the experiment are accounted for by Fourier-based first-order motion energy detection (van Santen & Sperling's [1985] elaborated Reichardt detector, which is based on Reichardt's [1961] motion detection model), as compared with the non-Fourier detection of counterchange (Hock et al., 2009). For both models, investigating shape judgments in addition to motion direction judgments requires addressing the spatial arrangement of motion detectors, in addition to their internal structure.

[2] The focus of this article is on the differential effects of figure displacement for same- versus inverted-polarity conditions. D_{max}, a measure of the maximum displacement for which motion is perceived, is not determined.

[3] Rather than focusing on the features of the space-time Fourier transform of the stimulus per se, our emphasis is on mechanisms proposed to *detect* Fourier-based motion energy—specifically, the elaborated Reichardt detector.

Experiment

The results of Sato's (1989) third experiment came closest to providing evidence for symmetry in direction discrimination for standard (same-polarity) and reverse-phi (inverted-polarity) motion. The possibility that this was due to ceiling effects for highly practiced observers was suggested by the lack of symmetry in his first two experiments, which used the same, although presumably less practiced, observers. In addition, in Sato's second experiment, the advantage in direction discrimination for standard motion, as compared with reverse-phi motion, became more pronounced when reducing the size of the elements lowered discrimination performance from ceiling.

The experiment closely resembles Sato's (1989) third experiment, in which participants indicated both the direction of motion and the shape of the displaced figure. In order to reduce the possibility of ceiling effects, testing was done primarily with naive participants who received minimal practice at the task and no feedback regarding the accuracy of their discriminations.

Method

Stimuli

The dynamic random checkerboard stimuli, which were generated with a Mac Mini computer, were centered in a Mitsubishi Diamond Pro 930SG monitor and viewed in a dimly lit room from a distance of 58 cm (maintained by a chinrest). As in Sato (1989), the stimuli were composed of two frames, each with a random checkerboard composed of 120 × 120 square elements that was presented against a black background. Each square element composing the checkerboards subtended a visual angle of 2 × 2 min (one pixel per check), and the entire checkerboard subtended a visual angle of 4° × 4°. The luminance of the white elements was 76.6 cd/m^2, and that of the black elements was 0.0 cd/m^2.

The first frame of each two-frame trial was generated by independently assigning each square element of the checkerboard to be either white or black, with a .5 chance of each. During the second frame, a region (the figure) was selected from the center of the first frame and displaced by 2, 4, 6, 8, 10, 12, 14, or 16 element-units (4–32 min) to the right or left. The rest of the checkerboard (the background) was randomly regenerated, again with a .5 probability of each element being white or black. The figure was either a vertically oriented rectangle (60 × 30 element-units; 120 × 60 min) or a horizontally oriented rectangle (30 × 60 element-units; 60 × 120 min). In the same-polarity condition, the luminance of the square elements composing the displaced figure was the same during both frames. In the inverted-polarity condition, the luminance of the square elements composing the displaced figure was inverted during the second frame; white elements became black and vice versa.

Procedure

To familiarize participants with the task, a version of the random checkerboard stimulus was shown in which all but the leftmost and rightmost two columns of elements from the entire 120 × 120 field of elements constituted the figure, which was displaced rightward or leftward by two element-widths (i.e., there was not an incoherent background from which coherent motion had to be segregated). In order to maintain the size of the field for the second frame, the two columns at the leading edge of the figure were removed rather than displaced, and the trailing two columns were randomly regenerated. This was done for both same- and inverted-polarity versions. Participants viewed these demos without feedback for approximately 5 min, until they indicated that they were able to perceive both leftward and rightward motions. Shape discrimination was then explained by means of drawings of the tall-thin and short-wide rectangles, and a demo stimulus composed of ten 138-ms frames, with two-element displacements during each frame (without polarity change). The figure shapes were easily discernible for this demo. A similar shape demo was not provided for the inverted-polarity condition, since it did not make the shapes discriminable and so did not aid in describing the task. Participants other than the first author received no practice with what would become the test stimuli.

As in Sato (1989), each test trial began with the participant fixating in the center of a 8 × 8 min square arrangement of four 2 × 2 min white dots, which was presented for 0.5 s against a black background. This was followed by a blank black screen for 0.5 s; then the two stimulus frames were presented for 138 ms each, and finally, another blank black screen was presented. After each trial, the participant made 2 two-alternative forced choice responses by pressing keys on the computer keyboard to indicate (1) the direction in which the figure was displaced (either right or left) and (2) the shape of the displaced figure (either a vertically or a horizontally oriented rectangle). There was no feedback.

Design

Blocks of 128 test trials were generated by the orthogonal combination of two displacement directions, eight displacement distances, two figure orientations, and four repetitions. Order was randomized within subblocks of 32 trials. The same- and inverted-polarity stimuli were tested in alternating blocks of trials. Each participant was tested for 7 blocks of trials for each polarity condition for a total of 14 blocks of trials.

Participants

In addition to the first author, 3 students from Florida Atlantic University voluntarily participated in this experiment. They were naive with respect to its purpose. All participants had normal or corrected-to-normal vision.

Results

The results for each of the 4 participants are presented in Fig. 2. Direction discrimination is graphed with respect to the actual figure displacement, regardless of the polarity condition. Thus, reverse-phi perception is indicated by responses that are systematically in the opposite direction of the displacement and, therefore, below chance level (i.e., below .5). As in Sato (1989), both direction and shape discrimination decreased with increasing displacement of the rectangular figure, with shape discrimination falling to chance at smaller displacements, as compared with direction discrimination. Most important, the results for each of the 4 participants indicated a clear asymmetry in both direction and shape discrimination between the same- and inverted-polarity conditions; both were superior in the same-polarity condition.

A two-way repeated measures ANOVA performed on the arcsine transformed proportion data indicated that the effects on direction discrimination of displacement size, $F(7, 21) = 55.74$, $p < .001$, luminance polarity (same or inverted), $F(1, 3) = 29.25$, $p < .05$, and the interaction between polarity and displacement size, $F(7, 21) = 14.37$, $p < .01$; all were statistically significant. (In the inverted-polarity condition, responses in the reverse-phi direction were treated as correct, so the complements of the proportion of correct responses were used in the ANOVA.) For shape discrimination, the effect of displacement size, $F(7, 21) = 11.93$, $p < .001$, and the interaction of polarity with displacement size, $F(7, 21) = 5.85$, $p < .01$, were statistically significant. For each participant, shape discrimination was better in the same- than in the inverted-polarity condition for the small displacements, but because of floor effects and the small sample size, the effect of polarity fell short of statistical significance, $F(1, 3) = 7.77$, $p = .069$.

Because there was a consistent trend of shape discrimination being better in the same-polarity condition for all participants, especially evident at the smallest displacement of two elements, a log-likelihood ratio test was performed for each participant, as well as their pooled scores, to evaluate the null hypothesis that the probability correct was identical in the two contrast conditions. That is, let p_S (p_D) be the proportion correct in the same-polarity (inverted-polarity) condition and p be the pooled proportion correct across both conditions; then the null hypothesis is $p_S = p_D = p$. If k_S (k_D) is the number of correct responses in the same- (inverted-) contrast condition and n_S (n_D) is the number of incorrect responses in the same- (inverted-) polarity condition, then the likelihood for the unconstrained model can be expressed as

$$LogLU = k_S \log(p_S) + n_S \log(1-p_S) + k_D \log(p_D) + n_D \log(1-p_D),$$

and the constrained model as

$$LogLC = (k_S + k_D)\log(p) + (n_S + n_D)\log(1-p).$$

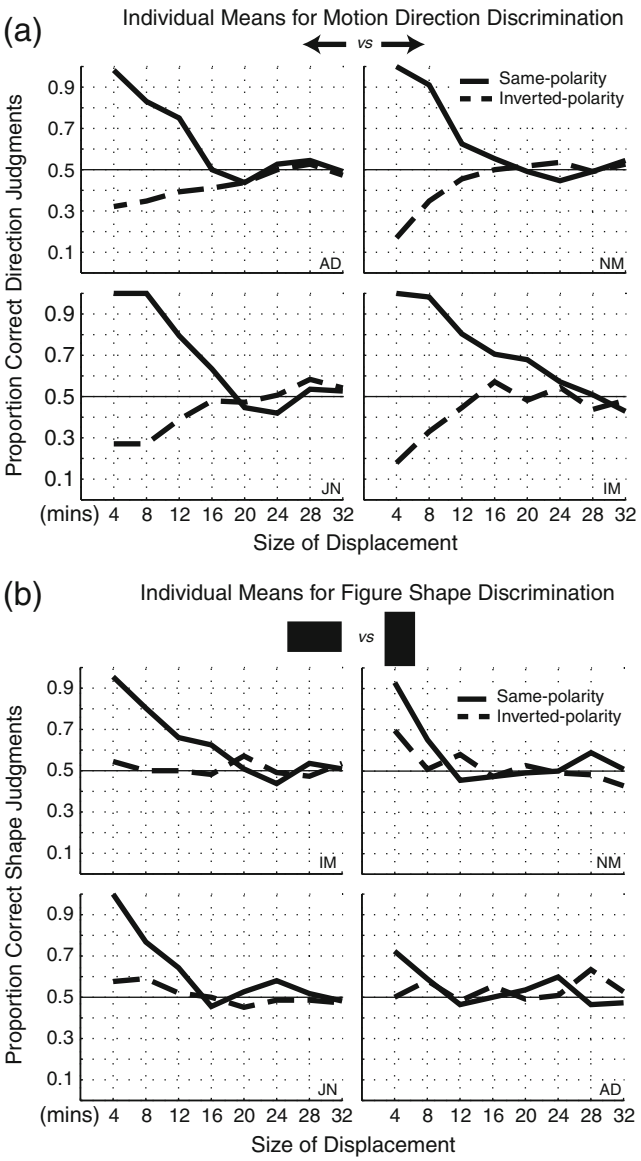

Fig. 2 Mean experimental results for individuals for **a** direction judgments (left or right) and **b** shape judgments (wide or tall rectangle). Proportion of correct responses are plotted as a function of figure displacement in dot-units. Solid lines indicate the *same-polarity* condition, and dashed lines indicate the *inverted-polarity* condition. Data points in panel a that are below chance (.5) indicate a systematic bias to see motion in the direction opposite to displacement (reverse-phi)

Then, under the null hypothesis $p_S = p_D = p$, the test statistic

$$X = 2(LogLU - LogLC)$$

is asymptotically distributed as chi-square with $df = 1$ (degrees of freedom determined by the number of free parameters in the constrained models subtracted from the number of free parameters in the unconstrained model). For each individual and for the pooled scores, the constrained (null) model was rejected in favor of the unconstrained model with $p < .001$ (with the greatest individual p-value = 4.4728×10^{-6}; individual chi-square values = 56.69, 57.28, 71.86, 21.05; pooled chi-square value = 123.39). These results suggest that the probability of a correct response in the same-polarity condition was significantly different from the probability of a correct response in the inverted-polarity condition at the displacement of two elements, for each participant individually and for their pooled responses.

If the effects on direction and shape discrimination were symmetrical, there would have been neither differences between the same- and inverted-polarity conditions nor significant interactions with the size of the figure displacement. Furthermore, the likelihood ratio test would have indicated no difference between the probability of a correct shape response in the same- and inverted-polarity conditions. The results indicate that this was not the case.

Computational simulations

Computational implementations of van Santen and Sperling's (1985) elaborated Reichardt detector (ERD) and Hock et al.'s (2009) counterchange detector, which are detailed in Appendix 1, were compared with respect to their ability to simulate the results of the experiment described above. For the purpose of these simulations, the two-dimensional random checkerboard stimuli were reduced to one-dimensional vertical bars whose luminance, white or black, was randomly determined, as was done by van Santen and Sperling (1985), Adelson and Bergen (1985), and Sato (1989). Consistent with the stimuli in the experiment described above, a portion of the random-bar stimulus was rigidly translated from the first frame to the second (the *figure*), while the rest of the stimulus (the *background*) was randomly generated in both the first and second frames. The stimulus was 240 bars long in the simulations. There were two figure lengths, analogous to the two figure shapes in Experiment 1: A figure that was 60 bars long represented the thin-tall rectangle, and a figure that was 120 bars long represented the wide-short rectangle. In the inverted-polarity condition, bars within the figure that were white during the first frame were black during the second frame, and vice versa. The figure was displaced by 2, 4, 6, 8, 10, 12, 14, or 16 bar-widths, the same displacements that were probed in the experiment. The *random bars* provided the input stimulus to the motion detector ensembles.

Coincidence detection and directional selectivity

Both models use the multiplication of activity patterns in pairs of spatially separated, one-dimensionalized edge filters (an excitatory zone and an adjacent inhibitory zone) to establish a correspondence between them.[4] However, the nature of the patterns whose coincidence is detected is different in the two models.

The ERD is sensitive to sequential changes in edge filter activation; that is, instantaneous edge filter outputs are compared at different points in time. This is achieved by delaying the output of one edge filter in order to temporally align activation that occurs at its location at one moment in time with the pattern of activation at a paired location at a later moment in time so that the patterns can be compared. At the level of the subunits where multiplication occurs (before the difference between the two subunits is taken), positive products signal motion from the location of the edge filter whose activity has been delayed to the location of the edge filter whose activation has not been delayed, while negative products signal motion in the direction from the location of the nondelayed edge filter to the delayed one.[5]

Although temporal coincidence is also central to the counterchange motion detector, a temporal delay is not required in order for it to be directionally selective. This is because the counterchange detector is sensitive to a particular pattern of simultaneous changes in edge filter activation: a decrease in the activation of one edge filter and a simultaneous increase in the activation of a paired edge filter. Rather than deriving a directional asymmetry from sequentiality, as in the ERD, an asymmetry in the direction of activational change in local spatial filters is established, with motion beginning from a location of a decrease in spatial filter activation and ending at a location of an increase in spatial filter activation. This is irrespective of the sequential order of the stimulus events producing the decreases and increases in activation (Gilroy & Hock, 2009; Hock et al., 2009).

[4] The scale of the edge filters for the ERD was determined by the quadrature constraint of the model. The edge filters for the counterchange model were selected to be most responsive to the size of the checks in the checkerboard stimulus.

[5] Typically, Reichardt-type detectors are described as detecting motion in the direction from the delayed input toward the nondelayed input. This, however, is not strictly true in the ERD formulation, since each subunit may carry information about two (opposite) motion directions (Adelson & Bergen, 1985; Lu & Sperling, 2001).

Edge filter polarity

In the ERD model, the multiplication of instantaneous outputs of the paired edge filters occurs irrespective of whether they are positive (excited) or negative (inhibited). On this basis, it is sufficient to have only one edge filter polarity for the ERD model (e.g., excitatory zone on the left, inhibitory zone to its right), since the entire range of positive and negative edge filter outputs take part in motion computation. In other words, both edge types are represented, one by positive values and the other by negative values. For example, if more white elements fall in the positive lobe than in the negative lobe of an edge filter during frame 1 (positive response) and more white elements also fall in the positive lobe of a paired edge filter during frame 2 (another positive response), the product of the two positive responses is positive. Furthermore, if more white elements fall in the negative lobe than in the positive lobe of the same edge detector during frame 1 (negative response) and more white elements fall in the negative lobe of the edge filter with which it is paired during frame 2 (another negative response), the product of the negative responses is also positive for the ERD. Thus, nothing would be added to the computations by including edge filters with reversed positive/negative polarity. It also is noteworthy that if a negative edge filter response in frame 1 is multiplied with a positive response in frame 2 (or vice versa), a negative response is elicited, indicating motion in the opposite direction than that of a positive response. Importantly, this is the basis for the ERD model signifying motion in the reverse-phi direction (although negative-valued products are also produced with non-inverted-polarity stimuli). These edge filter products occur at the level of the ERD subunits, from which the difference is taken to determine the final motion detector output.

In contrast, in the counterchange model, the activation values of edge filters are half-wave rectified, so only positive outputs are subject to the subsequent change detection that leads to motion detection. This is in line with the principle of counterchange motion pairing "like" edges, detecting their disappearance at one location and appearance at another location (this is discussed in more detail in the General Discussion section). For this reason, the model includes two edge filter polarities. The filter with its excitatory zone on its left side captures inputs in which there are more white elements falling on the filter's left side, whereas the filter with the excitatory zone on the right captures inputs in which there are more white elements falling on the filter's right side. The two edge filter polarities compute motion in parallel.

Opponency

The ERD is an opponent system; it takes a difference between its two component subunits for its final output. Each subunit can carry information about both leftward and rightward motion, because they each can have negative or positive values. Taking the difference between the subunits gives the final motion output. Net positive outputs signal motion in one direction (i.e., rightward) and net negative outputs in the opposite direction (i.e., leftward). Furthermore, opponency is necessary to prevent the ERD from signaling motion in response to stationary patterns. For purposes of comparing the two models, the counterchange model was arranged in a similar opponent fashion, with leftward motion signals being subtracted from rightward signals. This is not a necessity for the counterchange model because, unlike the ERD, leftward and rightward motion signals are separable and motion cannot be signaled for stationary stimuli. Therefore, by convention, rightward motion is represented in both models by positive values and leftward motion by negative values at each location along the detector arrays.

Spatial arrangement of motion detector arrays

For both ERD and counterchange motion detectors, the distance between the centers of the pair of edge filters that provide input to each motion detector is referred to as that detector's *span.* (This is illustrated in Fig. 3, which shows the general layout of both the ERD and counterchange detectors.) Both models included arrays of detectors with spans of two, four, six, and eight bar-widths. Within each array, the detectors densely covered the entire stimulus. Edge filters that served as

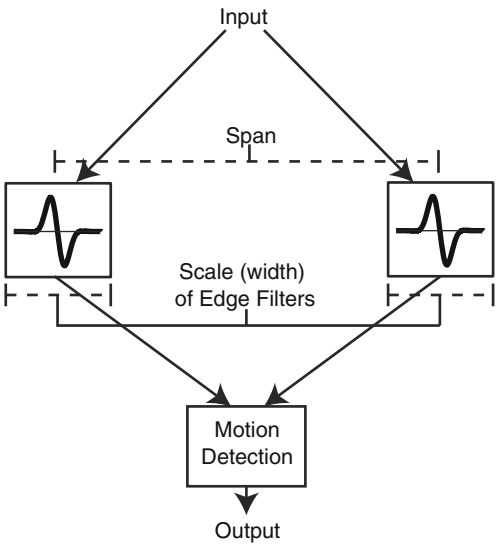

Fig. 3 General layout of both motion detectors. A pair of edge filters separated in space serve as inputs to subsequent motion detection; the distance between the centers of their respective fields is referred to as the detector's *span*. For the ERD, the size of the span and the scale (width) of the edge filter covary in order to maintain an approximate quadrature relationship (i.e., so there is approximately a 90° phase shift with respect to their preferred spatial frequency). The counterchange detector has no such constraint, and in the present model, the scale of the edge filters is held constant over a range of spans. For both models, detectors are arranged in layers, and each layter corresponds to a specific span

input to the motion detectors were located every one fourth of a bar-width across both the displaced figure and its background. Following van Santen and Sperling's (1985), there were multiple layers of motion detectors, each layer corresponding to a particular span. In the present simulations, this meant that there were four layers.

Direction discrimination

In order to simulate the direction discrimination task, for each trial, all motion signals were summed across space and across layers, and the sign of the sum indicated the motion direction decision (since rightward motions were positive and leftward motions were negative). Within each layer, responses were summed across all motion detectors covering the 240 random bars constituting the entire stimulus (not just the 60 or 120 random bars corresponding to the displaced figure). Summing activation over the entire field of random bars was significant because it meant that motion direction was being discriminated by the models without predetermination of the shape of the figure. That is, figure segregation was not considered a prerequisite for direction detection. This is consistent with the shape of the figure being derived from the motion rather than vice versa. Motion detector responses were also summed across all layers (spans). That is, all spans contributed equally to the determination of motion direction. This implies that direction discrimination does not depend on motion signals being concentrated at a particular span or in a particular image location.

For each trial, therefore, a positive sum (the positive component is greater than the negative component) signifies rightward motion perception, whereas a negative sum signifies leftward motion perception. In this way, both models make the same kind of forced choice responses as the participants in the actual experiments. The proportion of trials that motion perception was signified in the direction of the displacement was determined for 224 repetitions (matching the aggregated number of experimental trials for the 4 participants in the experiment). Proportions in the direction of the displacement that were less than .5 indicated that a majority of the simulated responses were in the so-called reverse-phi direction.

Shape discrimination

The ability of participants in the experiment to discriminate the shape of the displaced figure indicates that the detected motion could be used to segregate the figure from its background and determine its shape. This was simulated for both the ERD and counterchange models with templates that corresponded to the width of the two figures. The two templates functioned as filters whose inputs were the spatial distribution of motion signals along the stimulus array.

The simulations for the experiment were based on two principles of coherent motion supporting the perception of shape-from-motion. Accordingly, coherent motion arises from regions of activated motion detectors that (1) are in the same direction and (2) are of the same span. A high density of such signals within a template's positive area, as compared with its negatively weighted flanking regions, would result in a positive template output. The same-span constraint on motion coherence was consistent with the two-dimensional percepts elicited by the rigidly translating figures in the experiment. (The possibility of relaxing this constraint to account for recovery of depth information is addressed in the General Discussion section.) One template was composed of a positive interior region matching the relatively short one-dimensional size of one figure (60 bar-widths), and another template was composed of a positive interior region matching the relatively long one-dimensional size of the other figure (120 bar-widths). All the detected motions within the figure region were summed with equal positive weight. Negative regions flanking the positive interior regions extended to the boundaries of the random-bar stimulus, which was 240 bar-widths in length. All detected motions within the flanking regions were summed with equal negative weight. The templates were normalized such that their positive interior region integrated to 1 and their negative exterior regions integrated to −1. For each trial, the output of each template was determined for each direction (leftward and rightward) and for each of the four spans. The figure size (either long or short) with the greatest template response was taken as the shape decision for a trial. (As in the experiment, shape discrimination required forced choice decisions by the models.)

Simulations based on the elaborated Reichardt detector

A diagram of the ERD can be seen in Fig. 4a. As in van Santen and Sperling's (1985) ERD model, the edge filters in its present implementation model are band-pass. Space-time filters in the Fourier domain are approximated by establishing a quadrature relationship between pairs of filters constituting a motion detector. Thus, pairs of edge filters, implemented as one-dimensional real-valued Gabor filters, are modulated by sine waves that are 90° out of phase with one another. Larger spatial filters are therefore required to approximate the quadrature relationship among motion detectors whose component receptive-field centers are further apart (i.e., have larger spans).

Results

Single-trial simulations

As was indicated above, rightward motion was signified by positive values and leftward motion by negative values. In the

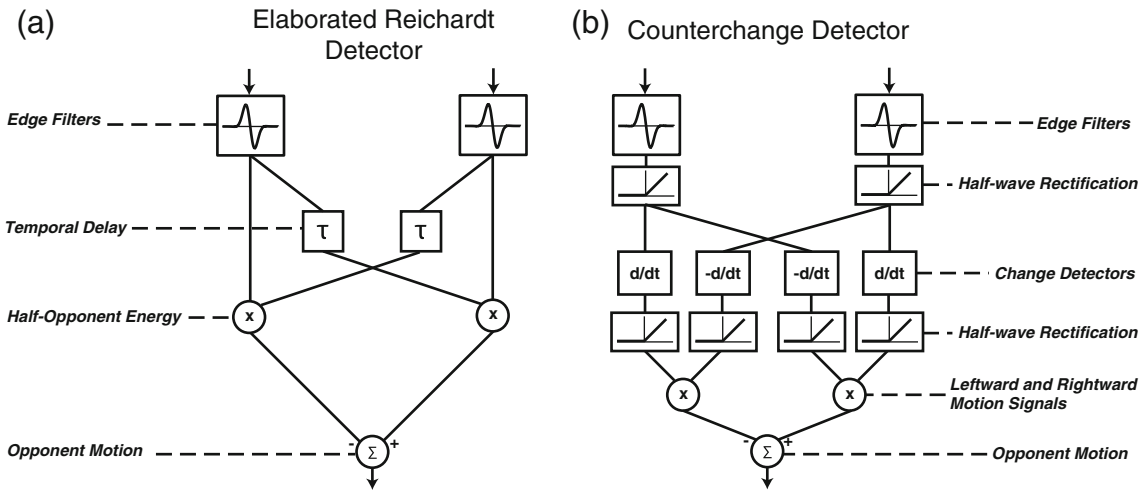

Fig. 4 Block diagrams of the **a** elaborated Reichardt detector and **b** counterchange detector. Only one polarity channel of the counterchange detector is shown here; the other one operates in parallel

single trials presented in Fig. 5, the displacement of the figure is to the right.

When the figure's displacement is small (e.g., 2 bar-units rightward; Fig. 5a), much of the activity is concentrated within the figure at the span that corresponds to the actual displacement, with most motion signals in the correct direction (rightward). In the background regions, there is also a fair amount of activity, although weaker on average and directionally incoherent, as would be expected for responses that are driven by noise. At larger spans, directional responses are generally consistent with the actual displacement direction within the figure region, but are spread across several spans for all displacement sizes, with the average strength of the response decreasing with greater spans. This weakening of the response is a consequence of the larger spatial filters required by larger-span detectors due to the ERD's quadrature constraint.

When the figure's displacement is larger (e.g., 6 bar-units; Fig. 5b), the span corresponding to the displacement shows a directionally consistent but relatively weak response within the figure region. The responses of nearby spans also are directionally consistent within the figure, and with similar strength. Therefore, the directional motion information for the figure region is again spread across several spans for all displacement sizes. Furthermore, small-span detectors that are driven almost entirely by noise respond strongly, due to their filters responding more strongly to the spatial structure of the stimulus.

Regardless of the size of the displacement, symmetrically opposite results were indicated for the inverted-polarity conditions when the second frame was the exact inverse of the second frame in the same-polarity condition. Motion was most often signaled in the leftward, reverse-phi direction within the figure, with the same strength and spatial distribution across all locations and spans, within both the figure and the background, as in the same-polarity condition (Fig. 5a, dashed curve).

Simulation of experimental results

ERD-determined simulations of direction and shape discrimination in the short-range motion paradigm are presented in Fig. 6a, b, along with the averaged results for the 4 participants in the experiment. It can be seen that the ERD successfully simulated the effect of displacement size; direction and shape discrimination were poorer for the larger displacements.

The ERD also simulates the perception of reverse-phi motion in the inverted-polarity condition but incorrectly predicts that it is quantitatively equal to motion in the direction of the displacement in the same-polarity condition; in the experiment, both direction discrimination and shape discrimination were significantly poorer for motion in the reverse-phi direction. It could be concluded, because of its inherent symmetry with respect to the same- and inverted-polarity stimuli, that the detection of first-order motion energy by the ERD is not sufficient in order to account for short-range motion perception.

Second-order motion energy

Also considered was the possibility that the perception of motion and shape entails second-order motion energy extraction (Lu & Sperling, 2001). Full-wave rectification of the edge filters' activation in the second-order system would make all negative activation values positive, so inverting luminance polarity would result in the output of the edge filters being the same as in the same-polarity condition. The simulation of second-order motion energy therefore would result in motion

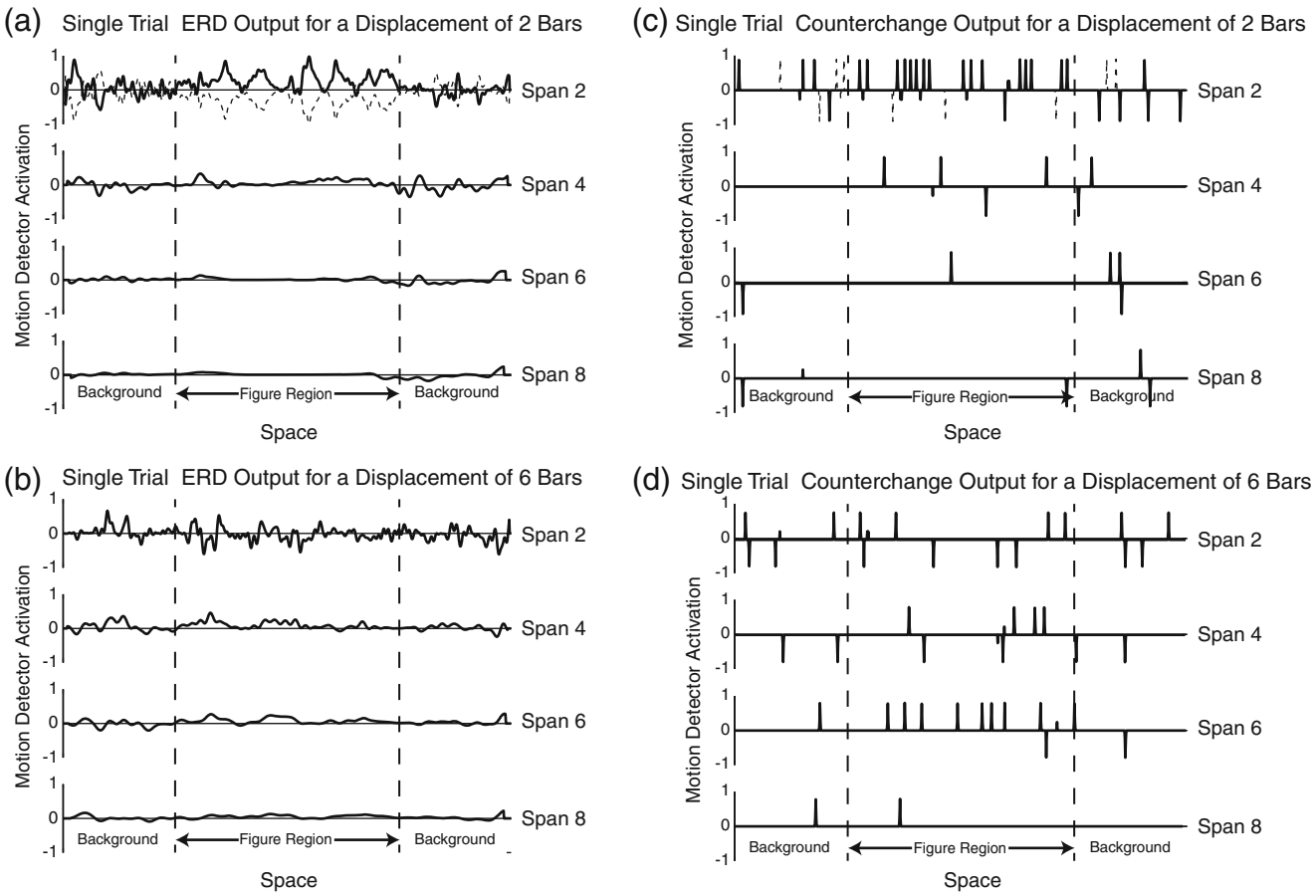

Fig. 5 Singlel-trial simulation outputs of the ERD (**a**, **b**) and counterchange detector (**c**, **d**). Panels a and d show a rightward displacement of 6 bar-units. Solid curves represent the local motion detector output across space for each of four layers of motion detectors with various spans. Activations above 0 signal rightward motion, and activations below 0 signal leftward motion. The figure occupies the region between the dashed vertical lines, and the flanking background regions fall outside of it. The dashed curve in the first detection layerin panels a and c depict the response to the inverted-polarity version of the same stimulus. Note the ERD's symmetry around 0 with respect to the same-polarity stimulus (reverse-phi). Although not depicted, the same symmetry is obtained for all the span-layers of the ERD. Also noteworthy is the indication that ERD activation is spread across span-layers, rather than being concentrated at the span corresponding to the displacement, particularly for larger displacements. In contrast, the inverted-polarity condition does not elicit a symmetric response from the counterchange detector. This is true at all span-layers, despite the dashed curve only being shown for the smallest span-layer in panel c

perception being signified in the direction of the displacement, regardless of whether or not the luminance polarity of the elements is inverted during the second frame of the two-frame trials. Reverse-phi motion percepts would not be predicted.

The effect of contrast

Van Santen and Sperling (1984, 1985) have reported that their experimental support for the ERD as the basis for motion perception was obtained only for low-contrast gratings. They argued that the perceptual invariance of suprathreshold motion is evidence of motion detectors' early saturation. It might be argued, therefore, that our empirical evidence, which was contrary to the predictions of the ERD, might have been due to testing short-range motion perception with high-contrast (black and white) elements. An experiment was therefore conducted in order to determine whether the ERD's prediction of symmetry with respect to the effect of same- versus inverted-polarity would be obtained at very low (barely visible) contrast levels. The results, which are presented in Fig. 7a, are very similar to those obtained in the primary experiment. That is, both better direction and shape discrimination were obtained for the same-polarity than for the inverted-polarity stimuli. A likelihood ratio test of the same form used to analyze the results of shape discrimination in the primary experiment was here used to test the significance of the difference in both direction and shape perception at the smallest displacement of 2 dot-units. For the direction discrimination task, the chi-square value was 90.18, $p < .001$; for

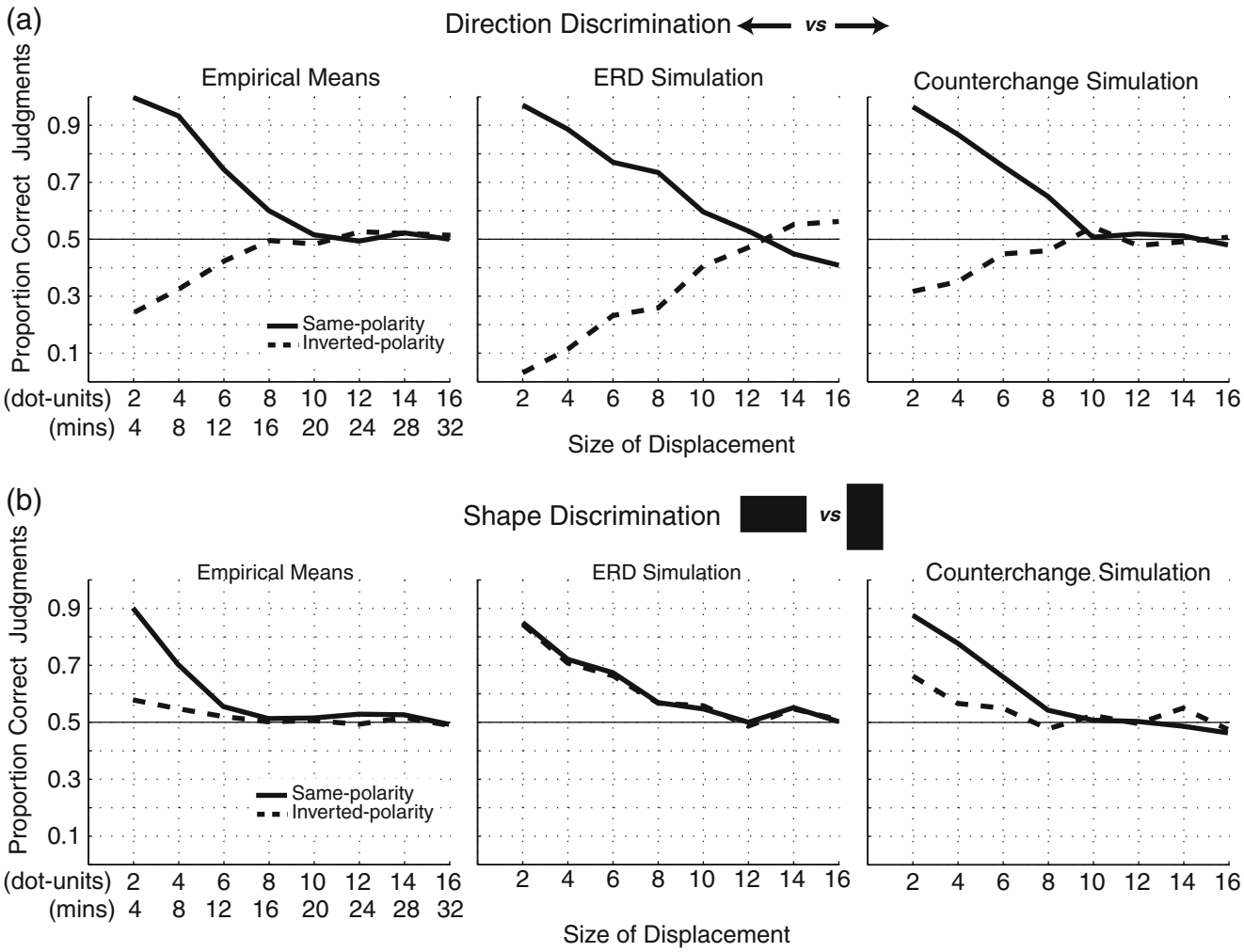

Fig. 6 Results from the experimental simulations alongside the empirical means for **a** the direction discrimination task (left or right) and **b** the shape discrimination task (wide or tall rectangle). Solid curves represent mean scores from the same-polarity conditions; dashed curves represent mean scores from the inverted-polarity condition. Because of symmetry in its response to the same- and inverted polarity stimuli, the ERD overestimates performance in the inverted-polarity condition for both direction judgments (corresponding to reverse-phi percepts) and shape judgments. The counterchange detector is very similar to the empirical data both qualitatively and quantitatively. The empirical symmetry between same- and inverted-polarity percepts as evidenced in both direction and shape judgments is clearly evident in the counterchange simulation

the shape discrimination task, the chi-square value was 319.81, $p < .001$. Symmetry with respect to luminance polarity was not obtained for low-contrast short-range motion stimuli, which might have been expected on the basis of van Santen and Sperling's (1984, 1985) evidence that the ERD functions properly only for low-contrast motion stimuli.

The effect of frame rate

Another possibility is that the ERD functions properly only for fast frame rates that more closely approximate continuous motion, so the lack of symmetry found in the main experiment may have been due to the relatively slow frame rate of the stimulus (138 ms/frame). A variant of the experiment was run with much faster frame rates (35 ms/frame). The same likelihood ratio test as in the low-contrast variant above was again run. For the direction discrimination task, the chi-square value was 69.29, $p < .001$; for the shape discrimination task, the chi-square value was 483.28, $p < .001$. Again, asymmetry with respect to polarity inversion was found for both direction and shape discriminations (Fig. 7b).

Simulations based on the counterchange motion detector

A diagram of the counterchange detector can be seen in Fig. 4b. The counterchange motion detector is sensitive to simultaneous and oppositely-signed changes in activation for pairs of spatial filters at separate locations (Hock et al., 2009), motion being signaled from the location of the decrease to the location of the increase in activation. Decrease subunits respond with excitation to decreases in their activational input, and increase subunits

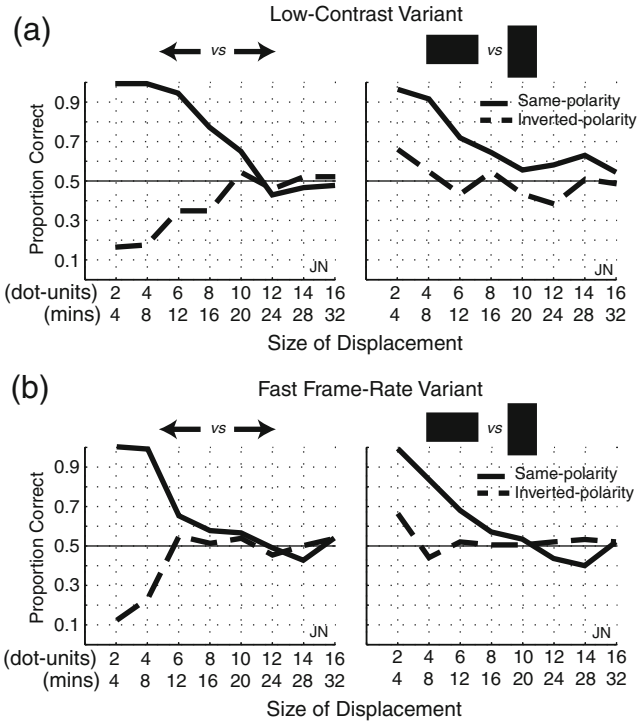

Fig. 7 Two varians of the experiment in order to test the effects of **a** low-contrast and **b** fast frame rates (35 ms) on the empirical asymmetry. Both conditions show the same asymmetry as the main experiment in both direction and shape judgments

respond with excitation to increases in their activational input. Counterchange-determined motion is indicated when the product of the "decrease" and "increase" excitation is greater than zero.

Although the perception of short-range motion has typically been attributed to the detection of motion energy (e.g., Adelson & Bergen, 1985; Cavanagh & Mather, 1989; van Santen & Sperling, 1985), it was shown by Hock et al. (2009) that it could plausibly be accounted for by the detection of counterchanging activation. Their account, which is recapitulated below, was based on the distribution of excitatory and inhibitory effects on spatial filters by the randomly arranged white and black elements constituting the short-range motion stimulus (Fig. 8).

Among the many edge filters that are stimulated by the figural portion of a random checkerboard, there are some that are (by chance) positively activated during the first frame of each two-frame trial (Fig. 8b). When the figure is displaced to a new location during frame 2, the filters that were excited during frame 1 will be stimulated by a distribution of elements that is more likely to produce a decrease than an increase in activation. (It is illustrated in Fig. 8a that there is a greater range of possible exCitation and inhibition levels that would lead to decreases, as compared with increases, in activation.) At the same time, the elements of the figure that had produced an excitatory effect on an edge filter during frame 1 are exactly displaced to a new location during frame 2, where they will produce similar activation of another, paired edge filter with the same excitatory/inhibitory polarity. It is likely that this filter was more weakly activated during frame 1, so its activation is likely to increase. A counterchange motion detector spanning these two locations within the figure will be activated by the multiplicative combination of decreased activation at one edge filter location and increased activation at another edge filter location. There is no constraint for the non-Fourier counterchange model that requires a quadrature relationship between the sizes of the edge filters and their span, so the size of the edge filters was the same for all spans.

As was indicated earlier, the outputs of the edge filters are half-wave rectified, so only positive activation levels are passed forward. Likewise, the outputs of the decrease and increase detectors are half-wave rectified before they are multiplied to yield a directionally-selective motion computation. The reasons for the inclusion of half-wave rectification after each stage of processing are twofold: for reasons of neural plausibility and for conceptual soundness of the counterchange principle. These issues are addressed in more detail in the General Discussion section.

In order to detect the motion of both white–black and black–white edges, two channels detect counterchange motion in parallel. One channel is responsible for edge filters with their excitatory zone on the left, and the other channel for those with their excitatory zone on the right. The motion computations for the two channels are then combined and the leftward signals subtracted from the rightward to yield a single array of motion responses.[6]

Finally, the counterchange model assumes that any decrease in edge filter activation can contribute to only one motion signal. Shorter-path motions beginning at the location of the activational decrease are preferred over longer-path motions, and in the case of conflicting directions of the same span, the stronger motion is preferred (in the case of equal strength, one motion or the other is chosen with an equal chance).

Results

Single-trial simulations

For small displacements (e.g. 2 bar-units rightward) in the same-polarity condition, rightward motions (in the direction of the displacement) were most strongly activated within the figure for the span corresponding to the size of the displacement (i.e., the motion signals were coherent; Fig. 5c).

[6] Although we used both polarity channels in the present simulation, virtually identical results are obtained when only one polarity channel is employed. However, because the ERD utilizes both edge polarities, a more direct comparison was achieved by including both channels. Additionally, including both channels shows that they do not interfere with one another.

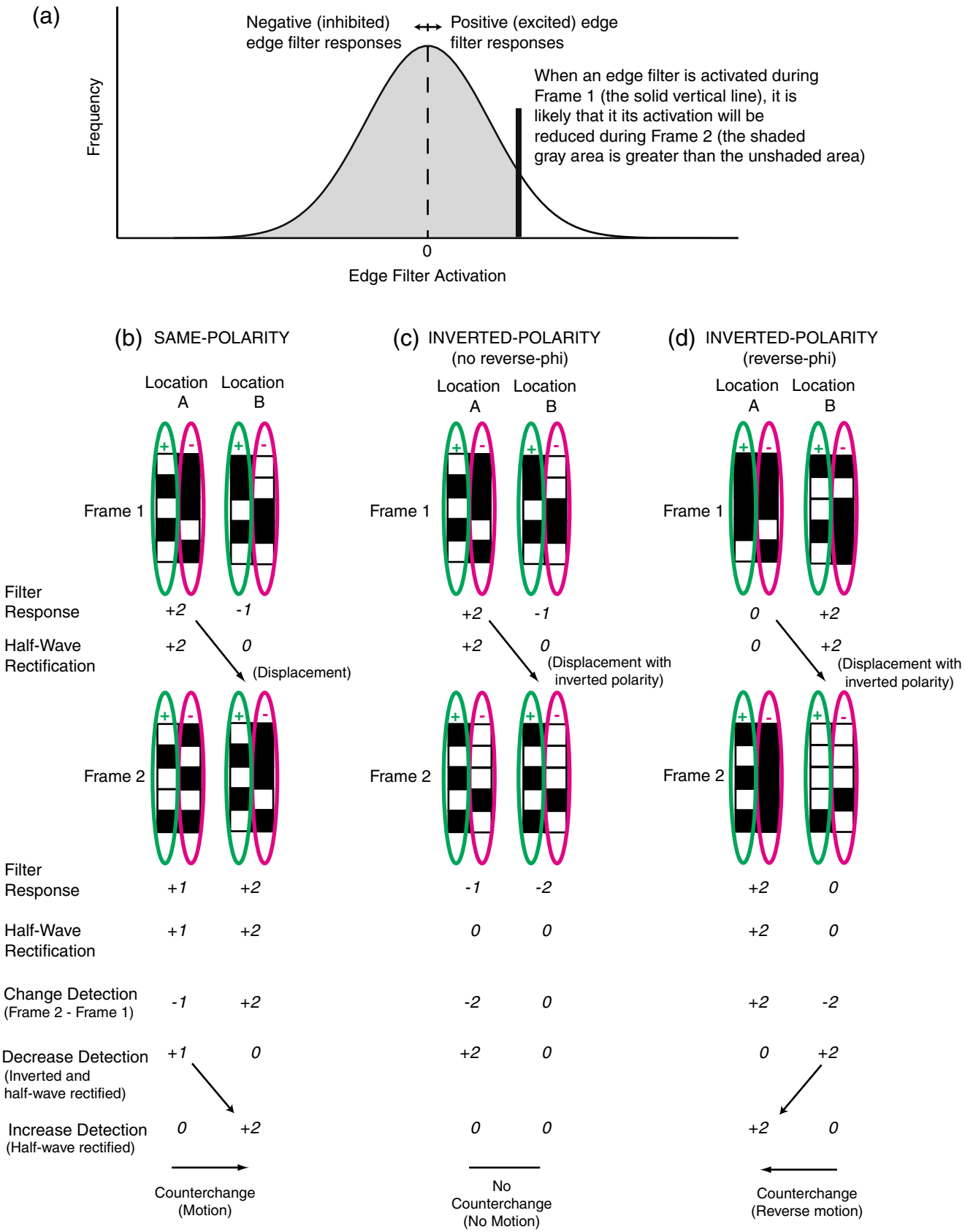
(a)
Negative (inhibited) edge filter responses
Positive (excited) edge filter responses
When an edge filter is activated during Frame 1 (the solid vertical line), it is likely that it its activation will be reduced during Frame 2 (the shaded gray area is greater than the unshaded area)
Frequency
0
Edge Filter Activation
(b) SAME-POLARITY
(c) INVERTED-POLARITY (no reverse-phi)
(d) INVERTED-POLARITY (reverse-phi)
Location A
Location B
Frame 1
Frame 2
Filter Response
Half-Wave Rectification
(Displacement)
(Displacement with inverted polarity)
Change Detection (Frame 2 - Frame 1)
Decrease Detection (Inverted and half-wave rectified)
Increase Detection (Half-wave rectified)
Counterchange (Motion)
No Counterchange (No Motion)
Counterchange (Reverse motion)

◀ **Fig. 8** Sketch of counterchange detection of motion in random-dot cinematogram, restricted to one polarity for simplification. **a** Illustration of why positively activated edge filters are likely to undergo a decrease in activation when the pattern is displaced out of their current location. For the same reason, there is likely to be an increase in activation at the location the pattern is shifted to. **b** Example of counterculture motion being detected for a stimulus in the same-polarity condition. **c** Typical nullification effects of polarity inversion on counterchange motion. **d** Arrangement of dots that elicit reverse-phi counterchange motion under polarity inversion

Responses in the background regions were sparser than in the figure, with inconsistent directionality.

For larger displacements (e.g., 6 bar-units; Fig. 5d), there was still activity within the figure region at the span corresponding to the displacement. However, it was less consistent than for the small displacements, with the distribution of motion responses spread across other, especially shorter, spans. Again, the background regions are sparsely activated and directionally incoherent.

In the inverted-polarity condition, motion signals were generally very sparse, both within and outside of the figure. At the span corresponding to the displacement, there are no motion signals generated within the figure in the displacement direction and a small number in the reverse direction. The latter skews the response distribution in favor of a leftward total response. This is indicated in Fig. 8c, d and is addressed in the General Discussion section.

Simulation of experimental results

The counterchange model does a very good job of simulating the averaged experimental results for direction and shape discrimination (Fig. 6a, b). It successfully simulates the effect of displacement size (both direction and shape discrimination were poorer for the larger figure displacements) and also simulates the weaker direction and shape discrimination obtained in the inverted-polarity condition.

These results contradict the general view that short-range motion is perceived via motion energy detection and that the perception of reverse-phi motion in particular is necessarily the result of motion energy detection. They show that a much different, non-Fourier model entailing the detection of counterchanging activation can fully account for both the perception of short-range motion and motion in the reverse-phi direction.

Spatial prefiltering

Whereas the scale of the edge filters for the ERD model were determined by the quadrature constraint of the model, the edge filters for the counterchange model were the same for all spans and were selected to be responsive to the intrinsic scale of the checkerboard stimulus. The filters for the counterchange model therefore were relatively small. Morgan (1992), however, has argued for a stage of spatial low-pass filtering prior to motion processing in order to account for how effects of displacement size vary with the size of the elements and the spatial frequency content of the image. Implementing this low-pass prefiltering did not produce major deviations from the simulation results obtained with the counterchange model without prefiltering. (This also was the case for the ERD model.)

General discussion

Any mechanism that yields symmetrical responses to same- and inverted-polarity two-frame stimuli cannot, by itself, account for asymmetrical data in either motion or shape discrimination for the short-range motion paradigm. In order for a motion detector to potentially account for the observed asymmetry, its polarity channels must either function in a completely segregated manner or contain a parameter that enables between-polarity interactions to be weighted differently than within-polarity interactions. The ERD, which in this article served as a representative model for the detection of first-order motion energy, does not segregate its polarity channels, nor does it contain a parameter that could weight the interactions of the polarity channels differently; therefore, it necessarily gives symmetrical responses to same- and inverted-polarity conditions. Moreover, symmetry with respect to polarity inversion is not unique to the ERD. It is intrinsic as well to Adelson and Bergen's (1985) motion energy detector, which replaces the multiplication scheme of the ERD by a sum-or-difference-then-square scheme. Despite such internal differences, it is formally equivalent on output to the ERD.

Both the ERD and the motion energy detector are comparator-type detectors that call for a quadrature arrangement of filters in order to approximate a region in the spatiotemporal Fourier domain. However, this quadrature arrangement is not a necessary condition for obtaining symmetrical responses to same- and inverted-polarity stimuli. Rather, the symmetry that these detectors exhibit results from treating both positive and negative spatial filter responses in the same manner; that is, the output values of spatial filters are treated arithmetically (e.g. multiplying negatives to get a positive response), rather than as representing a biophysical quantity in the nervous system. Consequently, when luminance polarity is inverted, the sign of the spatial filter response is also inverted but retains the same magnitude. Regardless of whether one uses the multiplication scheme of van Santen and Sperling's (1985) ERD or the sum-or-difference-then-square scheme of Adelson and Bergen's (1985) motion energy detector, this inversion of the local spatial filter responses on the second frame results in a change in the sign (direction) but not the magnitude (strength) of the final motion detection output,

leading to reverse-phi motion of equal magnitude to that in the same-polarity condition. Moreover, the symmetry that results from this multiplicative interaction is not unique to comparator-type detectors. Gradient detectors that evaluate motion at zero-crossings (Marr & Ullman, 1981) exhibit symmetry for the same reason. That is, inverting polarity on the second frame changes the sign of the temporal derivative, consequently inverting the sign of local motion signals while preserving their magnitude and spatial distribution (Sato, 1989). The contribution and interaction of negative values in comparator-type (and gradient) detectors raises questions with respect to their biological plausibility. Neural systems generally communicate via action potentials, where only positive activation is transmitted to postsynaptic units (Heeger, 1993). Inhibition of a neuron reduces the amount of output, but chemical synapses cannot transmit less-than-zero values. The less-than-zero contributions entailed in the ERD (and other models) makes a one-to-one mapping from the model to the nervous system doubtful, since negative values are not treated as inhibitory. In contrast, the counterchange detector, which successfully accounts for the asymmetrical effect of luminance polarity on direction and shape discriminations, is neurally plausible, since only positive activation values contribute to motion detection computations.

Source of asymmetry and reverse-phi in counterchange model

The half-wave rectification of edge filter outputs also is responsible for motion being asymmetric in the same- and inverted-polarity conditions. Because motion is computed within polarity channels and not between them, stimuli that would have signaled motion in the same-polarity condition in most cases have their motions nulled rather than reversed in the inverted-polarity condition. An example in Fig. 8 is restricted to one polarity channel for simplicity. In the same-polarity condition (Fig. 8b), a pattern of elements that is positively stimulating edge filter A in frame 1 is shifted to edge filter B in frame 2. This shift causes a decrease in response in A and an increase in response in B, signaling motion in that polarity channel from A to B. In the inverted-polarity condition (Fig. 8c, d), the response of B in frame 2 is necessarily of the opposite polarity. Its response is therefore negative, and the half-wave rectification leads to an output of zero. A zero output during frame 2 implies that over the course of the two frames at B, the only possible responses are a decrease or no response (i.e., there cannot be an increase to zero, since it is the lowest possible value for a half-wave rectified signal).

In the inverted-polarity condition, some arrangements of stimulus elements lead to counterchange detection in the direction opposite to displacement (reverse-phi motion). Figure 8d shows an example of such an arrangement. In frame 1, a near-zero response is elicited in an edge filter at location A, and a stronger positive response is elicited in an edge filter at location B. In frame 2, the near-zero response from location A has shifted to location B and been inverted, causing a decrease in activation (the inverted response of a near-zero output is also near-zero), while new elements are shifted into location A that happen to cause an increase in that polarity channel, eliciting a (reverse) counterchange response. This reverse-phi signaling is rare, as compared with counterchange detection in the same-polarity condition in the direction of displacement, since most responses are zeroed and do not lead to a reverse-phi signal. This leads to the observed asymmetry between same- and inverted-polarity counterchange detection.

Half-wave rectification in the counterchange model

Half-wave rectification at each stage of processing (only positive activation levels are passed forward) is an essential feature of the counterchange model. In addition to its previously discussed biological plausibility (a given neuron can transmit more or fewer action potentials, but never less-than-zero), half-wave rectification ensures that inhibitory activation states have no role in signaling the presence of counterchange, which entails a motion event that is detected by virtue of the (effectively) simultaneous *decrease* in a feature at one location and *increase* in that same feature at another location. In the present case, the features are white–black (and black–white) edges that are formed by chance within a random cinematogram; motion is signaled from the location of a *decrease* in edge filter activation to the location of an *increase* in edge filter activation. Such features can be (more or less strongly) present, or not present, but not negatively present.

Moreover, if half-wave rectification were removed prior to the detection of decreases and increases in spatial filter activation, the resulting negative values would introduce ambiguities into the conceptual framework of counterchange. For example, the response of a BW filter would be positive to a black–white (BW) edge, negative to a white–black (WB) edge, zero to a black–black (BB) nonedge, and zero to a white–white (WW) nonedge. If the BW edge filter is exposed to a two-frame sequence in which it is stimulated first by a WB edge, followed by a WW nonedge, its activation will have gone from a negative value to zero, so it would have *increased* (assuming no rectification). However, in order to conform to the principle of counterchange, this event is more appropriately registered as a *decrease* in the presence of a feature (WB edge), rather than as an increase in a feature (BW edge). Introducing half-wave rectification eliminates this ambiguity, treating the increase of a BW edge as nonsymmetrical with respect to the decrease of a WB edge (and vice versa). In other words, the increase in one feature does not imply an equivalent decrease in its polar opposite feature. By including separate channels for each of the polar opposite edge filters, what

would be a negative value for one channel (without rectification) constitutes positive values for the other channel.

Removing rectification before the outputs of the increase and decrease subunits of the counterchange detector are multiplied also leads to violations of the counterchange principle, eliminating directional selectivity. That is, instead of motion occurring exclusively from the location of a positive response for a decrease subunit to the location of a positive response for an increase detector, the opposite motion could also be signaled from the location of the activation increase because the negative output from a decrease detector (indicative of an increase in activation) can be multiplied by a negative output from an increase detector (indicative of a decrease in activation), yielding a positive motion detector output, erroneously signaling motion from an *increase* to a *decrease* in local activation.[7]

Dual motion pathways

It is well known that the nervous system is segregated into two parallel pathways that respond with excitation to opposite luminance-contrast polarities. The so-called ON and OFF channels respond to luminance increments and decrements, respectively. Here, we use the terms ON and OFF pathways to refer to two parallel channels opposite luminance polarity sensitivity and do not intend to imply a specific type of spatial filter (e.g., center–surround, edge detector, etc.). The two segregated polarity channels in the counterchange model can be interpreted as corresponding to these two pathways, each computing motion independently. Our simulations show that these two segregated counterchange channels (or either one by itself) are sufficient to account for both the standard and reverse-phi percepts in the current stimulus. Furthermore, other studies have shown evidence for the independence of these channels in computing motion by demonstrating similar asymmetries (e.g., Dosher, Landy, & Sperling, 1989; Edwards & Badcock, 1994; Sato, 1989; Wehrhahn & Rapf, 1992).

In contrast, the aim of Bours, Kroes, and Lankheet (2009), using a sparse random-dot display in which individual motion signals were spatially and temporally uncorrelated, was to show that motion detection thresholds were symmetrical for same- and inverted-polarity dot-pairs. They argued that this suggests that motion is computed by correlating (with equal weighting) signals both within and between the ON and OFF polarity channels, with between-channel correlations signaling reverse-phi motion. Such an architecture could account for the symmetry observed in the ERD without appealing to the interaction of negative activation values (an example of such a detector can be seen in Eichner, Joesch, Schnell, Reiff, & Borst, 2011).[8]

Although most of the parameter space probed in Bours et al.'s (2009) experiments was not indicative of symmetry (detection thresholds were higher for inverted-polarity stimuli), symmetry with respect to luminance inversion was consistently obtained for brief frame durations and small displacements. Because they also are the spatial and temporal conditions that are optimal for the perception of two-frame short-range motion (Braddick 1974), it is worth considering the implication of these results for motion detection. That is, they indicate that for fast motions over short distances, direction discrimination is based on a motion mechanism that correlates within- as well as between-polarity channels, which is implied by motion energy models. Furthermore, the spatially and temporally uncorrelated nature of the motion signals generated by Bours et al.'s (2009) stimuli implies that the integration of motion signals does not depend on their being simultaneous or spatially contiguous. In contrast, the short-range motion paradigm studied in the present article constrains coherent motion signals to occur simultaneously and within a spatially defined region (i.e., the displaced rectangle) where all dots undergo the same frame-to-frame translation. These conform to natural constraints of a rigidly translating surface, where motion signals are necessarily generated simultaneously and are in close proximity to one another by virtue of physical connectedness. Under these constraints, there is convergent evidence that spatial structure is not recoverable when luminance polarity is inverted, while it is recoverable when polarity is held constant. Evidence obtained in the present study, Sato's (1989), and Dosher et al.'s (1989) are consistent in indicating that same-polarity motion correspondences are essential for the perception of shape from motion.

Overall, these results are consistent with the existence of dual pathways, one entailing within-polarity counterchange mechanisms for the perception of motion for displaced objects, surfaces, and shapes, and the other entailing within- and between-polarity motion energy mechanisms for the

[7] It would be feasible to remove one of the rectifiers after change detection as long as the other was still present and achieve reasonable behavior from the detector; as long as the negative outputs of the motion detector were ignored and only positive outputs signal motion (if one channel can never go below zero, a positive product cannot result from multiplying two negative values). However, the motion-opponency scheme employed here to evaluate the final motion detection output would demand half-wave rectification on output of the motion detector, effectively displacing a rectifier, but not eliminating it.

[8] Eichner et al. (2011) have also presented a '"2-quadrant" Reichardt detector model in which only ON–ON and OFF–OFF spatial filter pairings are established to account for physiological findings in the visual system of the fly. This model showed weakened responses to inverted-polarity, as compared with, same-polarity, stimuli. However, it included front-end elaborations whose introduction is not currently justified for the human visual system. Nonetheless, it would be valuable for future studies to compare the response characteristics of this Reichardt-variant detector to the counterchange detector under conditions, which could clearly distinguish the models (i.e., stimuli in which no counterchange information is present but a clear autocorrelation is not, and vice versa).

perception of objectless global motion, without the individuation of particular objects, surfaces, and shapes.

The distinction between these two kinds of motion pathways has its origin in Wertheimer's (1912) distinction between beta (object) and phi (objectless) apparent motion. More recently, Sperling and Lu (1998) asserted that object motion entails the detection of motion via their third-order, salience-based motion system, whereas objectless motion is perceived when motion is signaled only by first- or second-order motion energy systems. Further evidence for dual pathways has come from Azzopardi and Hock (2011), who found that motion direction can be discriminated in the cortically blind hemifield of an individual with unilaterally damaged visual cortex (and thus, no object or shape perception) on the basis of detected motion energy, whereas motion direction was discriminated on the basis of changes in shape in the unimpaired hemifield. Finally, Hock and Nichols (2013) and Seifert and Hock (2014) have provided evidence linking the perception of a surface's motion with the detection of counterchange and the detection of changes in luminance (without the perception of surface motion) to the detection of motion energy.

It is likely that these two motion systems, sensitive to different stimulus patterns, subserve different behavioral functionalities—for example, the counterchange pathway to perceive changes in position of objects and the motion energy pathway to perhaps detect optic flow patterns that guide locomotion (Pelah et al., 2014). The motion energy pathway, which leverages both within- and between-polarity-channel correlations, subserves *global* motion perception, while the counterchange pathway, detecting only same-polarity patterns, subserves *form*/*motion* perception, which can include the derivation of a figure's shape from the spatial relationships among counterchange-determined motion signals (Fig. 9). Further empirical work to identify the spatial and temporal limits for the perception of spatial structure in the counterchange pathway and to determine what, if any, spatial localization is possible in the motion energy pathway would help to further distinguish these two systems.

To summarize, several speculative conclusions can be drawn from the relevant literature:

1. Although asymmetry in motion direction discrimination between same- and inverted-polarity stimuli is observed under most experimental conditions, evidence for symmetry is obtained for very fast motions over small distances in Bours et al. (2009). This parameter range is typically associated with the short-range paradigm, suggesting that the presence of spatial structure among motion signals, which is absent in Bours et al.'s paradigm but present in Braddick's (1974) short-range paradigm, can affect motion detection. The evidence for symmetry obtained by Bours et al. is consistent with motion energy as the basis for motion direction discrimination in the absence of spatial structure.
2. The presence of temporal simultaneity and spatial contiguity among motion signals is not necessary to obtain asymmetry with respect to luminance inversion; for example, Bours et al. (2009) have obtained evidence for asymmetry with a stimulus for which motion signals are spatially and temporally uncorrelated (this was the case for slow motions over relatively long distances). However, when simultaneity and spatial contiguity are present, as in the short-range motion paradigm, asymmetry with respect to luminance inversion is obtained (as in the present study) even when fast motions are perceived over small distances (see Fig. 6b).
3. Spatial structure and form, including depth structure, is recoverable only in same-polarity conditions (likely through the detection of counterchange) and is decimated in inverted-polarity conditions (Fig. 2 in the present study; Dosher et al., 1989; Sato, l989).
4. To the extent that ON and OFF channels (or other opposite-polarity channels) are correlated in motion detection, local spatial relationships are lost, and the motion percept could be called *global*. Spatial and temporal pooling in the motion energy pathway could be responsible for this loss (as suggested by the nature of the Bours et al. [2009] stimulus).

The source of shape from coherent motion

The dual-pathways dichotomy described above proposes that the detection of counterchange is basis for the derivation of shape from coherent motion that has been defined as occurring when multiple motion detector responses agree in direction and span. When there is a high density of coherent motion signals within some region of the moving image, that portion of the image is perceived as moving together as a continuous "surface." In order to segregate the moving surface from the background, coherent motion signals must be relatively dense within the figure and relatively sparse and/or incoherent outside the figure. This difference in coherence and density between the moving figure and the background is essential for successful segregation and the recovery of shape, since it is the only cue to the boundary of the figure.

This definition of coherence is at odds with how coherence is typically framed in terms of motion energy (Sato, 1989; Simoncelli & Heeger, 1998). The general motion energy approach entails taking local velocity estimates of oriented sinusoid components across a dynamic image. The output of a given motion detector is then considered a time-varying velocity estimate at a given location, where the sign of the output signifies the direction of motion and the magnitude signifies the speed. In this view, multiple motion signals across some

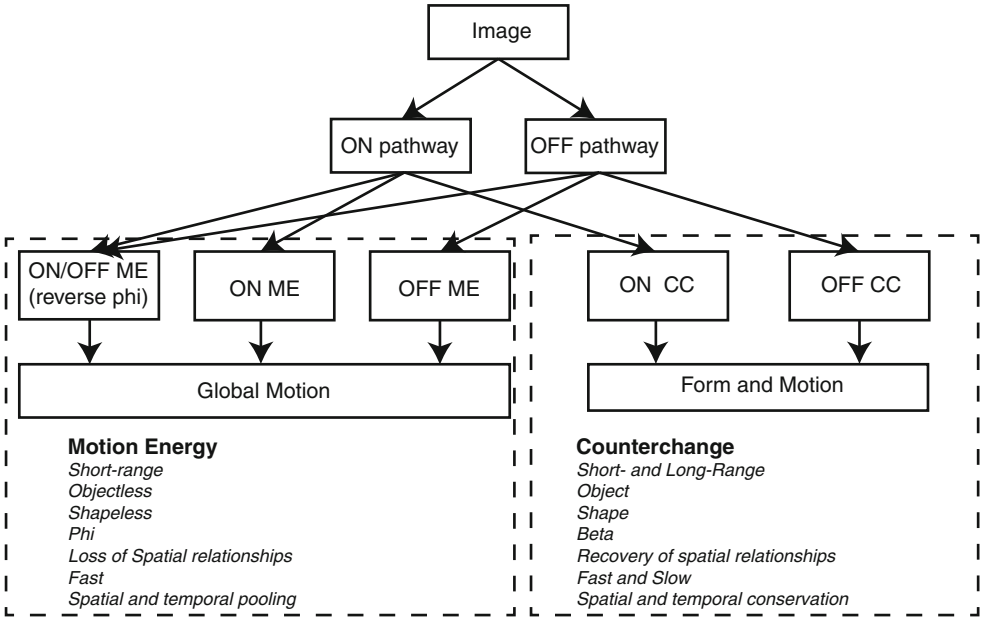

Fig. 9 Conceptual model of a dual-pathway motion system. ON and OFF here designate two channels with opposite luminance-polarity sensitivity and do not necessarily imply a particular type of spatial filter. Both within- and between-polarity interactions subserve a motion energy (ME) system that detects global motion. Only within-polarity interactions subserve a counterchange (CC) system in which spatial relations of motion detectors are preserved, allowing for recovery of form from motion

area of the image would be considered coherent if their direction and *speed* were sufficiently similar (Yuille & Grzywacz, 1998). In other words, among motion detectors of the same scale and directional selectivity, a low variance across the response magnitudes (speeds) would constitute evidence of coherent motion. This presents a challenge for the ERD account of shape-from-motion for short-range motion stimuli. For small displacements, single-trial simulations for ERD detectors (Fig. 5a) indicate strong directional agreement, but with a high degree of variance in terms of magnitude (and therefore, speed).[9]

The present approach using the counterchange detector assumes a different role of motion detector responses. Rather than the magnitude of the response representing a velocity estimate, detector responses are conceived of as providing evidence for a given displacement (corresponding to the span of the detector). While the phase-invariant responses of motion energy detectors signal luminance-defined motion at a single location, counterchange detectors signal motion of an image feature (e.g., an edge) from one location to another. A strong motion detector response indicates strong evidence for a given displacement corresponding to the detector's span. Weaker responses, which could occur for multiple reasons (pattern details, smaller contrast change, etc.), are not indicative of slower speeds but, instead, provide reduced evidence of motion between two locations. There are two consequences of this approach: (1) Counterchange-determined motion marks spatial distances, providing a direct basis for the recovery of shape from motion, and (2) rather than a homogeneous (i.e., low-variance) response magnitude across a given direction and span, a sufficient density of responses for a given span is required for coherence within an image region.

While the interpretation of the outputs of ERD and counterchange detectors differ in general, in the present article, they both simulate shape judgments with the same template-matching scheme. This scheme does not take into account the variance of motion detector magnitudes, and the criterion for coherence is the same for both models.

Theoretical framework for the recovery of depth from counterchange motion

Although the definition discussed above limits motion coherence to motions of the same direction and span, this restriction can be relaxed to account for coherent motion patterns that give rise to the impression of depth structure in moving images. The framework follows from the idea that motion direction and shape discrimination entail patterns of activation within and across layers of motion detectors with the same directional selectivity, with each layer composed of a spatially distributed, densely packed array of motion detectors. The defining feature for each layer is that the same span separates the pairs of edge filters that compose its constituent detectors.

When the directionally consistent motion detector activation within a displaced surface is concentrated in a particular span-layer, it indicates that the detected motions all are in the same depth plane, as must be the case for two-dimensional surfaces oriented perpendicularly with respect to one's line-of-sight. However, if motion signals within some local neighborhood occur at different, but similar, span-layers, these motions

[9] Sato's (1989) motion-energy-based computations of shape-from-motion invoke a secondary "directed matching" algorithm, in addition to a motion detection algorithm, in order to minimize the variance. Spatial pooling in Sato's model might also lead to a lower overall variance, but at the cost of deteriorating spatial resolution, which is likely to be necessary for figure segregation.

may be interpreted as belonging to a single surface that is nonuniform in depth. For example, if a one-dimensional slice were taken along the direction of motion from the front face of a rotating cylinder composed of moving dots, all the dots would be moving in the same direction but would stimulate different span-layers depending on the speeds of the dots (the speeds are constrained by the three-dimensional structure of the cylinder). Dots near the outer edges of the cylinder would be moving relatively slowly, therefore activating small-span detectors. Toward the center of the cylinder, the speed of the moving dots would increase, leading to the activation of larger-span detectors, with a maximum span reached at the center. With a sufficient density of dots, this cross-layer activation pattern would be smooth, with neighboring detectors differing only minimally in span. Templates similar to the ones used in the present simulations for single-depth motion could respond to sufficiently smooth patterns across span-layers, signaling depth structure in the moving image.

The single-trial simulations in Fig. 5, which were the basis for the discrimination of motion direction and shape in the short-range motion paradigm, made it possible for the counterchange model and the ERD motion energy model to be compared with respect to their compatibility with this theoretical framework for deriving depth structure from image motion. Two features of the simulations are relevant: (1) the extent to which motion detector activation for displaced surfaces is concentrated within the same span-layer and (2) the spatial resolution of the activation patterns.

Concentration of activation within a span

It can be seen for the ERD simulations in Fig. 5 that directionally consistent motion is most strongly concentrated within the displaced surface for the detector span that corresponds to the surface's displacement. However, directionally consistent activation is evident for other spans. The latter occurs because the ERDs are Fourier-based, so their edge filters are constrained to maintain a quadrature relation between filter size and span. As a result, the detectors composing different span-layers overlap significantly in terms of their spatiotemporal frequency response. Thus, a motion detection response in a given layer is likely to be accompanied by similar responses in layers with similar spatiotemporal frequency sensitivities (i.e., with similar spans). Because of the Fourier character of motion energy detectors like the ERD, this sort of diffusion across multiple span-layers is unavoidable for most displaced objects.

This "muddling" of span-layer activation for the ERD does not occur for the counterchange model, because directionally consistent motions are concentrated within the displaced surface only for the detector span that corresponds to the surface's displacement (particularly for small displacements). Because the counterchange model does not require a quadrature relationship between the span and size of the edge filters composing the motion detectors, detectors have the same size edge filter for every span. The consequence is that the spatiotemporal stimulus patterns that a detector is sensitive to are more dissimilar across span-layers than for the Fourier-based ERD. Because the edge filters for each span respond to the same stimulus information, the detectors whose span corresponds to the actual figure displacement will generally signal more strongly and more often than displacement-inconsistent spans. In addition to this, the shortest-path selection constraint in the counterchange simulation minimized further the incidences of multiple motion signals occurring across multiple span-layers at a given location.

Spatial resolution

It also can be seen in Fig. 5 that essentially all ERD detectors composing a span-layer are activated for virtually every location across the short-range motion stimulus, regardless of whether the detectors' edge filters are responding to changes in element luminance occurring within the displaced figure or within the background. In contrast with this spatially continuous distribution of activation, the distribution of counterchange detector activations within the figure is dense but discontinuous, and outside the figure, responses are very sparse (Fig. 5c). This is due to the counterchange detectors being much more selective than the ERD motion energy detectors (and not to the difference in spatial filter inputs to the two models). That is, counterchange detectors are responsive to a much smaller number of random dot patterns than are motion energy/comparator models like the ERD. This is because counterchange detectors are activated only when their edge filters are affected by changes in element luminance that result in decreases in edge filter activation at one location and increases in edge filter activation at another location, whereas nearly any change in edge filter response will result in a motion signal for the ERD. A discontinuous but dense distribution of activated motion detectors is important for the spatial resolution of the shapes that are derived from detected motion, especially when such a pattern indicates depth structure. That is, recovering depth would be exceedingly difficult if it were unclear which span-layer was optimally stimulated at a given location, since the relation between neighboring motion signals at different spans would need to be differentiated in order to discern differences in depth.

Conclusion

In this article, we have demonstrated the insufficiency of comparator-type motion energy detectors such as the ERD in accounting for motion direction perception and shape-from-motion segregation in the short-range motion paradigm. As an

alternative, we have shown the plausibility of a counterchange-based mechanism in accounting for these experimental results. It is argued that the detection of counterchange-determined motions mark spatial distances, providing a direct basis for the perception of spatial shape from motion. In addition, we have suggested how counterchange detection could be extended to account for the recovery of depth from motion. Finally, non-Fourier counterchange detection can potentially account for other phenomena (e.g., the correspondence problem) that do not conform well to motion-energy formulations without necessitating high-level token trackers or centralized cost–function calculations (Dawson, 1991; Morgan, 1992).

Appendix 1. Computational simulations

Stimulus

The stimuli, each consisting spatially of 240 bars and temporally of two frames, are defined as S(x,t) at all locations along the stimulus array x = [1 960]. Each random bar is composed of 4 pixels), with each location taking on the value 0 (representing black) or 1 (representing white) and t = 1,2 (representing frames 1 and 2). A central figure region (either 60 or 120 bars long) is translated to the right by 2, 4, 6, 8, 10, 12, 14, or 16 bar-widths from frame 1 to frame 2, while the background regions are independently and randomly generated for each frame.

Edge filters

One-dimensional real-valued Gabor functions (a Gaussian window modulated by a sine function) are used for all spatial filtering in both the ERD and counterchange detectors. The function is centered around zero and uses a 0-phase sine-wave modulator so that it serves as a balanced receptive field by virtue of it being antisymmetrical around zero. The filter is described by the equation $g(x)$ below. Parameter σ sets the standard deviation of the Gaussian window, and parameter p sets the period of the sine wave modulator (in dot units). The ratio between the two parameters is the same in all edge filter instantiations, regardless of scale (p/σ = 5). Finally, edge filters are normalized such that their positive lobes always are integrated to 1 and their negative lobes to −1.

$$g(x) = w(x,\sigma)c(x,p)$$
$$w(x) = e^{-\frac{x^2}{2\sigma^2}}$$
$$c(x) = \sin\left(2\pi\cdot\frac{1}{p}\cdot x\right)$$

Implementation of the ERD (Fig. 4a)

Four scales of edge filters are used for the ERD simulation. This is necessary in order to approximate quadrature for motion detectors with differing spans (i.e., distance between the center of the receptive fields that serve as inputs to a motion detector). Parameter values are listed below, with subscripts indicating layer numbers, with layers 1, 2, 3, and 4 corresponding to motion detectors with spans of 2, 4, 6, and 8 bars, respectively.

$$p_1 = 8; p_2 = 16; p_3 = 24; p_4 = 32$$
$$\sigma_1 = 1.6; \sigma_2 = 3.2; \sigma_3 = 4.8; \sigma_4 = 6.4;$$

For each motion detector layer, the entire one-dimensional stimulus is convolved with the corresponding edge filter kernel (convolution being notated by *) for both frames (here notated with the index i). The result is truncated at both ends to maintain the original stimulus size:

$$r_i(x) = g(x) * S(x,i).$$

For each location along the detector array a motion signal $m(x)$ is calculated by

$$m(x) = r_1(x)r_2(x+x') - r_1(x+x')r_2(x),$$

where $r_i(x)$ is the edge filter response at location x for frame i and x' is the magnitude of the detector span corresponding to a given motion detection layer. The resulting array is padded with zeros in order to maintain the one-to-one correspondence between the motion detector array and the stimulus.

Implementation of the counterchange detector (Fig. 4b)

Only one scale of edge filter was used for the counterchange detector, regardless of the span. The parameters were

$$p = 2; \sigma = .4.$$

Both frames of the stimulus are convolved with the edge filter. In a computational shortcut, two polarity channels are derived from the filter response by half-wave rectifying the filter responses to form channel 1 and inverting and half-wave rectifying the responses to form channel 2.

Half-wave rectification:

$$h(x) = \begin{cases} x & when > 0 \\ 0 & when \le 0 \end{cases}$$

Channel 1 responses for frames i = [1,2]:

$$r_{1i}(x) = h(r_i(x))$$

Channel 2 responses for frames i = [1,2]:

$$r_{2i}(x) = h(-r_i(x))$$

The frame-to-frame change in filter response is calculated as

$$c_c(x) = r_{c2}(x) - r_{c1}(x),$$

where subscript c stands for channel c = [1,2] and the second subscript refers to the frame index.

Decrease and increase responses for each channel are calculated by taking the half-wave rectified change values for the increase response and inverting and half-wave rectifying for the decrease responses:

$$i_c(x) = h(c_c(x))$$
$$d_c(x) = h(-c_c(x))$$

For each location along the detector array of a given span, motion is computed for both channels and summed into a single motion vector:

$$m(x) = \sum_{c=1,2} d_c(x) \cdot i_c(x + x') - d_c(x + x') \cdot i_c(x),$$

where x' equals the span of a given layer. Motion response arrays are padded with zeros in order to maintain correspondence with the stimulus. Finally, motion responses over a threshold (.2 in the reported simulations) inhibit longer range motions originating from the same decrease locations (i.e., the inhibited motions are set to 0). If two motions sharing a decrease location are of the same span but opposite directions, the stronger response is taken and the other set to 0, or else for equal strength motions one is selected with a .5 probability and the other set to 0. Thresholding prevents near-zero responses from contributing to inhibitory interactions, but the exact size of this threshold did not have much effect, since individual counterchange responses tended to be very vigorous or very weak (i.e., well above or well below threshold). These interactions serve as a weak shortest-path assumption in the counterchange model (weak because splitting motions are prevented, but converging motions are not).

Direction decisions

After each trial, for each of the two detector arrays (ERD and counterchange), the motion responses are summed across all locations and spans. Rightward motion was signified by positive values, and leftward motion by negative values.

Shape decisions

Two templates that corresponded to the 2 one-dimensional figures are used to make a shape decision, long versus short line, after each trial. The templates consist of an interior positive region that corresponds to the figure sizes (60 and 120 bars) and flanking negative regions that extended to the edge of the stimulus. The value is homogeneous across the interior region (i.e., the same at all locations) and, likewise, is homogeneous across the flanking regions. The interior regions were normalized such that they integrated to a value of 1, and the flanking regions are normalized to integrate to a value of −1. After a trial, rightward and leftward motions for each detection layer are separated in order to assess their template response independently (leftward motions were made positive so that only positive responses were considered as template matches). Each span-layer (separated by direction) is correlated with both templates. The corresponding figure of the maximum template response is taken as the shape decision for a given trial.

Appendix 2 Symmetry of elaborated Reichardt detector to two-frame same- and inverted-polarity stimuli

Consider a two-frame stimulus J in which frame 1 is some spatial function $f(x)$ and frame 2 is some other spatial function $g(x)$. A *point-delay* Reichardt detector exposed to stimulus I can then be described as

$$R_{x_1,x_2,\delta_t}[I](t) = I(x_1, t-\delta_t)I(x_2, t) - I(x_1, t)I(x_2, t-\delta_t)$$

where x_1 and x_2 are the two points in space that the detector is sensitive to and $\boldsymbol{\delta}_t$ is the delay used to detect motion across the two points. In response to the two-frame stimulus J, $R_{x_1,x_2,\delta_t}[J](t)$ will be zero, except for those ts during frame 2 for which frame 1 was on at time $t-\delta_t$. For all such ts,

$$R_{x_1,x_2,\delta_t}[J](t) = f(x_1)g(x_2) - f(x_2)g(x_1).$$

Now consider the inverted-polarity version of the same stimulus K with the same first frame $f(x)$, but in which spatial function of the second frame $h(x)$ is the opposite of $g(x)$:

$$h(x) = -g(x)$$

$$\begin{aligned} R_{x_1,x_2,\delta_t}[K](t) &= f(x_1)h(x_2) - f(x_2)h(x_1) \\ &= f(x_1)(-g(x_2)) - f(x_2)(-g(x_1)) \\ &= -(f(x_1)g(x_2) - f(x_2)g(x_1)) \end{aligned}$$

Thus,

$$R_{x_1,x_2,\delta_t}[K](t) = -R_{x_1,x_2,\delta_t}[J](t).$$

Furthermore, Chubb and Sperling (1988) proved that the response of any Reichardt detector with arbitrary spatial and temporal filters can be expressed as a linear combination of

point-delay Reichardt detector responses. This implies that the response of any given Reichardt detector, regardless of its spatial or temporal sampling characteristics, is the negative of the detector's response to an otherwise identical two-frame stimulus in which the luminance polarity of the second frame is inverted. This is true regardless of whether or not the two frames represent a spatiotemporally shifted pattern (i.e., motion) or not (i.e., noise).

References

Adelson, E. H., & Bergen, J. R. (1985). Spatiotemporal energy models for the perception of motion. *Journal of the Optical Society of America A, 2*(2), 284–299.

Anstis, S. M. (1970). Phi movement as a subtraction process. *Vision Research, 10*(12), 1411–1430.

Azzopardi, P., & Hock, H.S. (2011). Illusory motion perception in blindsight. *Proceedings of the National Academy of Sciences, 108*, 876–881.

Bours, R., Kroes, M., & Lankheet, M. J. (2009). Sensitivity for reverse-phi motion. *Vision Research, 49*(1).

Braddick, O. (1974). A short-range process in apparent motion. *Vision Research, 14,* 519–527.

Cavanagh, P., & Mather, G. (1989). Motion: The long and short of it. *Spatial vision, 4*(2–3), 2–3.

Chubb, C., & Sperling, G. (1988). Drift-balanced random stimuli- A general basis for studying non-Fourier motion perception. *Optical Society of America, Journal, A: Optics and Image Science, 5,* 1986–2007.

Dawson, M. R. (1991). The how and why of what went where in apparent motion: Modeling solutions to the motion correspondence problem. *Psychological review.*

Dosher, B. A., Landy, M. S., & Sperling, G. (1989). Kinetic depth effect and optic flow–I. 3D shape from Fourier motion. *Vision Research, 29*(12), 1789–1813.

Edwards, M., & Badcock, D. R. (1994). Global motion perception: Interaction of the ON and OFF pathways. *Vision Research*.

Eichner, H., Joesch, M., Schnell, B., Reiff, D. F., & Borst, A. (2011). Internal structure of the fly elementary motion detector. *Neuron, 70*(6), 1155–1164. doi:10.1016/j.neuron.2011.03.028

Gilroy, L. A., & Hock, H. S. (2009). Simultaneity and sequence in the perception of apparent motion. *Attention, Perception & Psychophysics, 71*(7), 1563–1575. doi:10.3758/APP.71.7.1563

Heeger, D. J. (1993). Modeling simple-cell direction selectivity with normalized, half-squared, linear operators. *Journal of Neurophysiology, 70*(5), 1885–1898.

Hock, H. S., Gilroy, L., & Harnett, G. (2002). Counter-changing luminance: A non-Fourier, nonattentional basis for the perception of single-element apparent motion. *JOURNAL OF EXPERIMENTAL PSYCHOLOGY HUMAN PERCEPTION AND PERFORMANCE, 28*(1), 93.

Hock, H., Schöner, G., & Gilroy, L. (2009). A counterchange mechanism for the perception of motion. *Acta Psychologica, 132*(1), 1–21.

Hock, H. S., & Nichols, D. F. (2013). The perception of object versus objectless motion. *Attention, Perception, & Psychophysics, 75*(4), 726–737.

Lu, Z. L., & Sperling, G. (2001). Three-systems theory of human visual motion perception: Review and update. *Journal of the Optical Society of America A, Optics, image science, and vision, 18*(9), 2331–2370.

Marr, D., & Ullman, S. (1981). Directional selectivity and its use in early visual processing. *Proceedings of the Royal Society B: Biological Sciences, 211*(1183), 151–180. doi:10.1098/rspb.1981.0001

Morgan, M. J. (1992). Spatial filtering precedes motion detection. *Nature, 355*(6358), 344–346. doi:10.1038/355344a0

Pelah, A., Barbur, J., Thurrell, A., & Hock, H.S. (2014). The Coupling of Vision with Locomotion in Cortical Blindness. *Vision Research,* (in revision).

Reichardt, W. (1961). Autocorrelation, a principle for the evaluation of sensory information by the central nervous system. In W. A. Rosenblith (Ed.), *Sensory Communication* (pp. 303–317). Cambridge: MIT Press.

Sato, T. (1989). Reversed apparent motion with random dot patterns. *Vision Research, 29*(12), 1749–1758.

Seifert, M.S., & Hock, H.S. (2014). The Independent Detection of Motion Energy and Counterchange: *Flexibility in Motion Detection. Vision Research,* (in revision).

Simoncelli, E. P., & Heeger, D. J. (1998). A model of neuronal responses in visual area MT. *Vision Research, 38*(5), 743–761.

Sperling, G., & Lu, Z.-L. (1998). A systems analysis of visual motion perception. *High-level motion processing, 153–183*.

Stevens, M., & Merilaita, S. (2009). Animal camouflage: Current issues and new perspectives. *Philosophical Transactions of the Royal Society B: Biological Sciences, 364*(1516), 423–427. doi:10.1098/rstb.2008.0217

van Santen, J. P., & Sperling, G. (1984). Temporal covariance model of human motion perception. *JOSA A, 1*(5), 451–473.

van Santen, J. P., & Sperling, G. (1985). Elaborated Reichardt detectors. *Journal of the Optical Society of America A, Optics and image science, 2*(2), 300–321.

Wehrhahn, C., & Rapf, D. (1992). ON- and OFF-pathways form separate neural substrates for motion perception: Psychophysical evidence. *The Journal of Neuroscience*, 1–4. Retrieved from http://www.jneurosci.org.ezproxy.fau.edu/content/12/6/2247.full.pdf

Wertheimer, M. (1912). Experimental studies of the perception of movement (Experimentelle Studien über das Sehen von Bewegung). *Zeitschrift für Psychologie under Physiologie der Sinnesorgane, 61,* 161–265.

Yuille, A. L., & Grzywacz, N. M. (1998). A theoretical framework for visual motion. In T. Watanabe (Ed.), *High-level motion processing* (pp. 187–211). Cambridge: The MIT Press.